12th International Symposium on Turbulence and Shear Flow Phenomena (TSFP12)
Osaka, Japan (Online), July 19-22, 2022

DATA-DRIVEN MODEL FOR VORTEX LOCK-IN OF CIRCULAR CYLINDERS IN AN ACOUSTICALLY-DRIVEN OSCILLATORY FLOW

Girish K. Jankee, Srikar Yadala, Eirik Æsøy, James R. Dawson & Nicholas A. Worth
Department of Energy and Process Engineering
Norwegian University of Science and Technology
Trondheim N-7491, Norway
Girish.K.Jankee@ntnu.no

ABSTRACT

The concept of vortex lock-in for a single circular cylinder in an oscillating flow, induced through acoustic forcing, is revisited over the second instability region. Multiple cylinder diameters are investigated over a Reynolds number range between 500 and 7200. The lock-in behaviour is inspected, both quantitatively and qualitatively, through hot-wire anemometry and planar particle image velocimetry (PIV) measurements. Initial results corroborate previous findings describing the frequency range over which lock-in is inherent for single cylinders. Additionally, the influence of the cylinder location in a standing wave (velocity node or pressure node) is observed to heavily influence the lock-in behaviour. A novel scaling which describes the onset of lock-in is subsequently established. This data-driven model demonstrates the necessity to account for the Strouhal number in predicting the velocity fluctuations required to achieve lock-in over the second instability region. Velocity fields also reveal the existence of bimodal shedding (symmetric or alternate) during lock-in, which can be associated to the non-dimensional groups present in the scaling. Finally, the occurrence statistics of each shedding pattern is found to be sensitive to the amplitude of the velocity fluctuations.

INTRODUCTION

Understanding the characteristics of vortex shedding is of paramount importance due to its ramifications in domains such as the structural design of heat exchangers, offshore platforms or bridges and instability control of flames (Sumner, 2010). While many aspects of the physics of vortex shedding from bluff bodies have been well established, there are still many scenarios where the impact of vortex shedding is less explored and understood. In this paper, we investigate vortex shedding off a single circular cylinder in the presence of acoustic forcing.

Disturbances can be added via controlled vibrations of the cylinder or through velocity fluctuations which can be generated by upstream flaps, active grids or by acoustically modulating the flowfield with electromagnetic speakers (Williamson, 1985; Barbi *et al.*, 1986; Hall *et al.*, 2003). In the latter case, Blevins (1985) demonstrated that a sound field (standing wave) could alter the motion of particles and induce vortex shedding at a frequency which fully correlated with the excitation frequency of the standing wave. Such a phenomenon is termed vortex lock-in and occurs when the vortex shedding frequency (f_s) of the cylinder is shifted from its natural state (f_0) and becomes half of the excitation frequency (f_e). While Barbi *et al.* (1986) reported a range of the lock-in envelope between f_e/f_0 of 1 and 2 (second instability region), other studies such as Al-Mdallal *et al.* (2007) and Konstantinidis & Balabani (2007) have found this range to extend to 3 or the existence of another lock-in regime around f_e/f_0 of 4 respectively. The amplitude of the acoustic forcing/oscillations has been associated with the existence of these multiple lock-in modes.

This lock-in behaviour can be further explored through an analysis of the topological features of the structures present in the wake of the cylinder. An extensive study by Detemple-Laake & Eckelmann (1989) characterised vortical structures across the second instability region as (i) being independent of f_e/f_0, (ii) formed upon synchronisation, i.e., lock-in at $f_s = \frac{1}{2}f_e$ or (iii) occurring at $f_s = f_e$. Flow visualisation revealed a kaleidoscope of patterns induced by the velocity fluctuations, which included but is not limited to symmetric, alternate (Kármán vortex street), vortex strings and isolated vortex pairs. Identifying the type of vortical structures present across the lock-in range is key in understanding the physical mechanisms responsible for lock-in. However, this has proven to be a complex task as is illustrated through the DNS results of Balachandar *et al.* (1997), where a cylinder had the same shedding frequency at f_e/f_0 of 2 in both a steady and an oscillating flow, but the observed vortex dynamics were different.

While multiple vortex patterns exist, a myriad of experimental and numerical studies have revealed that the perturbations across the flow direction during lock-in can be primarily associated to two types of vortex shedding: alternating and symmetric modes. Konstantinidis *et al.* (2005) noted that the alternating mode corresponds to the 2S mode (classical Kármán vortex street), while the symmetric mode resembles the 2P mode. The alternating mode generally occurs when the incoming flow is steady while Konstantinidis & Liang (2011) have shown that in symmetric modes, the flow perturbations promote the simultaneous formation of vortices in the shear layer roll-up on both sides of the cylinder. This implies that the symmetric mode is synchronised with the oscillatory component. The type of mode present depends on the amplitude of the flow perturbations. At low values, the alternating mode is predominant and even when the symmetric mode occurs, the shed vortices are unstable and break down within a few downstream diameters, giving rise to an anti-symmetric arrangement (Konstantinidis & Balabani, 2007).

Moreover, both Ongoren & Rockwell (1988) and Konstantinidis *et al.* (2007) observed a bimodal behaviour during

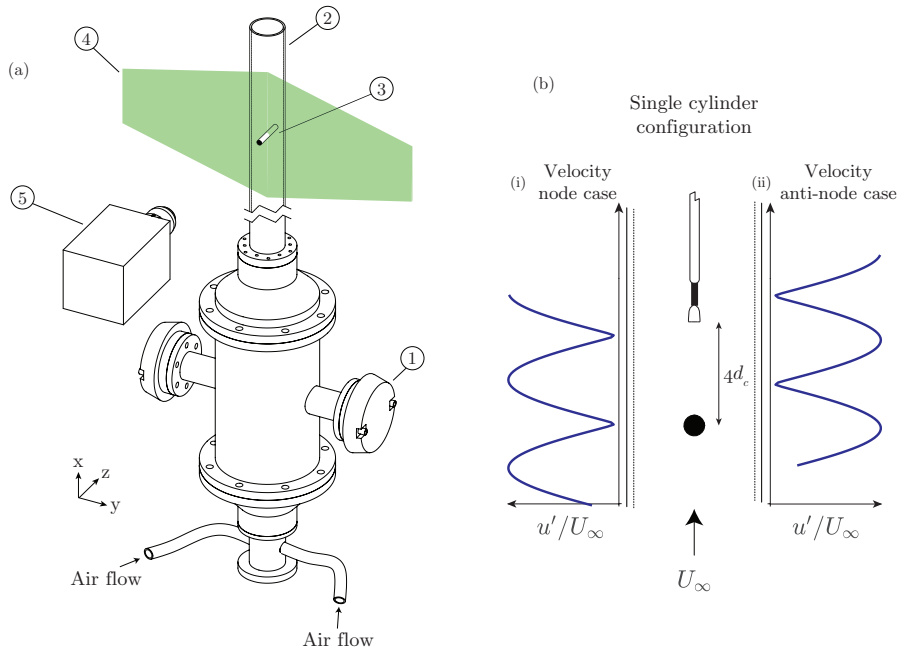

Figure 1. (a) Schematic of the experimental setup (not to scale), with the following components: 1. *Monacor KU-516* loudspeakers, 2. Test-section pipe, 3. Cylinder, 4. Laser sheet, 5. PIV camera, (b) Single cylinder at (i) velocity node location and (ii) velocity anti-node location, with the hot wire probe positioned $4d_c$ downstream

which there was a competition and switching between the alternating and the symmetric modes in the near wake. Konstantinidis *et al.* (2007) noted that this switching between the modes was random but the number of occurrence of each mode was found to be a function of the excitation frequency, the amplitude of the perturbation as well as Reynolds number of the incoming flow. The existence of this bimodal behaviour highlights the ambiguous nature of the flowfield during lock-in and demonstrates that the physical mechanisms responsible for lock-in are yet to be fully understood. Furthermore, although there is significant evidence which highlights a conjunction between the amplitude of oscillations, viz. velocity fluctuations, and the vortex lock-in regime, the absence of any scaling to capture this behaviour is remarkable. This article primarily aims to establish such a scaling through a systematic parametric study by revisiting the concept of vortex lock-in for a single circular cylinder in an oscillating flow. Additionally, the flow fields of the cylinders' wakes are examined under conditions of lock-in with the aim of complementing existing explanations on the mechanisms driving lock-in.

EXPERIMENTAL SETUP

The experimental setup is shown in figure 1. The test-section was made from a 560 mm long acrylic pipe with a diameter of 35 mm and the flow into the test rig was monitored and regulated using an *Alicat* mass flow controller with a maximum range of 1000 slpm and accuracy of $\pm$2.5 slpm. A *TTi-40 MHz* waveform generator was used to create a sinusoidal waveform for driving the loudspeakers. The flow was forced acoustically at frequencies of 730, 1460 and 2190 Hz, which corresponded to standing wave modes of the pipe, while the amplitude was varied by adjusting the input voltage. At 730 Hz, a velocity node and anti-node of the acoustic mode were located at 150 mm and 270 mm from the pipe exit respectively (see figure 1(b)). These corresponded to the cylinder locations studied in this paper. The cylinder diameters, d_c, were 1.7, 2.0, 2.4, 4.0 and 6 mm. The amplitude of the velocity fluctuations at the velocity anti-node was controlled through pressure measurements with Bruël and Kjær 1/4" condenser microphones at four different axial locations and using the multiple microphone method of Seybert & Ross (1977). The forcing amplitude (u'/U_∞) was varied between 0 and 30 %. The cylinder-based Reynolds number (Re) of the flow was altered between 500 and 7200 to change the natural shedding frequency of the cylinder and thus, vary f_e/f_0 between a range of 1 to 2.5.

Firstly, hot-wire anemometry measurements were performed with a single-wire traversing hot wire probe of diameter 5 μm and prong spacing 1.25 mm which was operated in constant temperature mode. The probe was aligned such that the wire was positioned at the center of the pipe and at a downstream distance of $4d_c$. Calibration of the hot-wire probe was performed using a jet with a top hat velocity profile with velocities ranging from 0-30 m/s. Following analysis of the hot-wire measurements, planar PIV (both high speed and low speed) was performed for selected cases to capture the dynamics of vortex shedding. These cases corresponded to f_e/f_0 of 0.7, 1.4 and 2.0 and u'/U_∞ of 7.5 and 15 % for the 1.7 mm cylinder diameter. The high speed imaging setup (HS) consisted of a Phantom V2012 1MP camera fitted with a 200 mm focal length lens and a Litron LDY300 high speed laser. 6000 image pairs were acquired at a rate of 3 kHz. The low speed PIV setup (LS) consisted of a Lavision imager LX 16 MP camera, also fitted with a 200 mm focal length lens and extension rings, and a Litron 200 mJ dual-pulse Nd:YAG laser. For this configuration, the laser and camera were phase locked to the excitation frequency signal at 12 equidistant phases. For each phase, 200 image pairs were recorded. Vector fields were determined using Lavision Davis 10 software. For the HS cases, an initial step with a window size of 64 × 64 px with an overlap of 50 % was applied followed by two passes of 24 × 24 px with a 50 % overlap. This resulted in a resolution of 0.236 mm per vector in both the x and y directions. For the LS cases, an initial step with a window size of 64 × 64 px with an overlap of

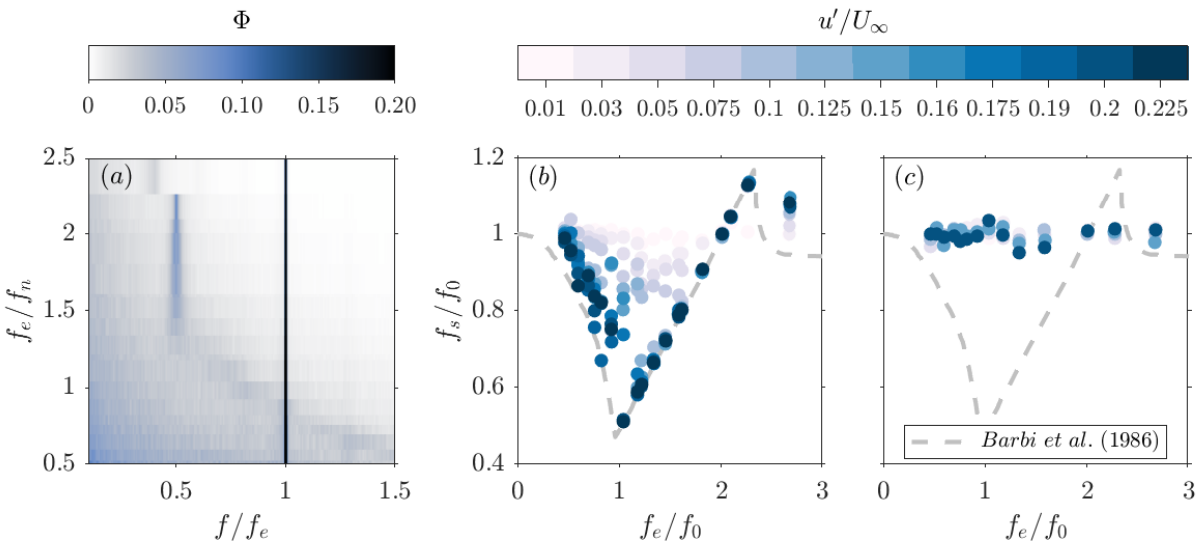

Figure 2. (a) Contour plot of the power spectra for an example case showcasing peak detection of dominant frequencies at lock-in. Plot of the vortex shedding frequency of the 2 mm cylinder, f_s, against the excitation frequency, f_e, both normalised by its natural shedding frequency, f_0, at (b) velocity anti-node and (c) velocity node, as the amplitude of the velocity fluctuations at the velocity anti-node is varied.

50 % was applied followed by two passes of 32 × 32 px with a 75 % overlap. This resulted in a resolution of 0.046 mm per vector in both the x and y directions.

RESULTS

Scaling of vortex lock-in

Hot-wire anemometry data was first analysed to determine the dominant frequencies present in the flow. The natural shedding frequency of the cylinder was first detected at each *Re* through identification of the most energetic peak in the power spectra, with the flow unforced. This also showed that the Strouhal number for the cylinders tested varied between 0.18 and 0.25. In the presence of acoustic forcing, two peaks emerge from the power spectra, corresponding to f_e and f_s (figure 2(a)). By tracking the evolution of f_s with *Re*, the lock-in characteristics of the cylinder can be quantified as displayed in figure 2, where the 2 mm cylinder was located at (b) the velocity anti-node and (c) the velocity node. Figure 2(b) shows the variation of f_s/f_0 with f_e/f_0 as the forcing amplitude is increased, with the dashed line representing a mean fitting curve from Barbi *et al.* (1986). Initial observations demonstrate that the lock-in behaviour of the single cylinder at the velocity anti-node corroborates well with the limits identified by Barbi *et al.* (1986). The lock-in envelope ranges from f_e/f_0 of 1 to 2.2, similar to the findings of Barbi *et al.* (1986) and Al-Mdallal *et al.* (2007). However, the f_e/f_0 range tested in this study is not deemed exhaustive enough to assess the occurrence of multiple lock-in modes, as ascertained by Konstantinidis & Balabani (2007). Note that for brevity, only the 2 mm case is shown in figure 2 but all d_c tested exhibited comparable behaviour.

Figures 2(b) and 2(c) also highlight the influence of the cylinder location on the lock-in characteristics, in the presence of a standing wave. At a velocity node, lock-in is nonexistent. Such a trend arises since in a standing wave, the velocity fluctuations are at their apogee at the velocity anti-node and zero at the node. Thus at a node, while pressure oscillations are large, the cylinder is only exposed to the mean incoming flow velocity and vortex shedding occurs solely at f_0. This is evident in figure 2(c), where the amplitude of the velocity fluctuations is always defined at the velocity anti-node. Therefore, while this parameter increases, the corresponding amplitude at the velocity node is consistently abated, resulting in a cylinder positioned at the node not experiencing lock-in. This confirms that the intensity of the velocity fluctuations is an important parameter in dictating the lock-in behaviour of the cylinder.

Additional insight into lock-in can be achieved by analysing the frequency ratio (f_e/f_0) corresponding to the onset of lock-in ($f_s/f_0 = 0.5$), for each amplitude of the velocity fluctuations at the velocity anti-node. From figure 3(a), the analysis of lock-in onset points for multiple cylinder diameters demonstrates a reasonable collapse and suggests the possibility to derive a universal scaling. As a first attempt, it is possible to try and fit the data points according to the equation below:

$$\frac{u'}{U_\infty} = A\left(\frac{f_e}{f_0}\right)^n. \tag{1}$$

Following non-linear regression, the values of constants *A* and *n* were found to be 0.23 and -2.68, respectively, with the r.m.s error of the fit equivalent to 0.13. Such a moderate value in the r.m.s error implies that equation 1 does not fully capture the non-dimensional groups relevant in describing the relation between u'/U_∞ and f_e/f_0. Therefore, a similar methodology as the one employed by Jankee & Ganapathisubramani (2021) is used to fit the scaling parameters to dimensional variables. The values of u' corresponding to the onset of lock-in are fitted against dimensional parameters defined in equation 2, after which the non-dimensional groups are formed using the coefficients obtained through the non-linear regression procedure (table 1). This method avoids any bias as fitting the scaling parameters against predefined non-dimensional groups, such as f_e/f_0 and u'/U_∞ only, limits the results to these assumed groups.

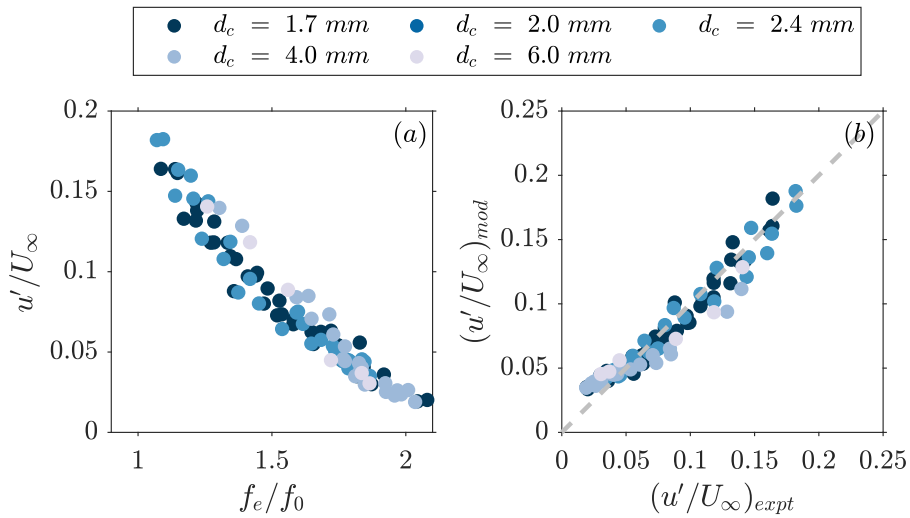

Figure 3. (a) Experimentally acquired data points describing the onset of lock-in for multiple values of f_e/f_0, prior to scaling, and (b) Comparison of u'/U_∞ corresponding to the onset of lock-in between experimental data $(u'/U_\infty)_{expt}$ and predictions by the data-driven model $(u'/U_\infty)_{mod}$.

$$u' = \mathscr{F}(f_0, f_e, U_\infty, d_c) = \lambda {f_0}^a {f_e}^b {U_\infty}^c {d_c}^d, \tag{2}$$

where λ is a constant and a, b, c and d are exponents obtained from non-linear regression.

Table 1. Fitted coefficients and normalised residual for the scaling of u' corresponding to the onset of lock-in and f_0. The 95 % confidence interval limits (CI_{95}) for the fitted parameters are also provided in the brackets.

	λ	a	b	c	d	$\varepsilon_{r.m.s}$
	0.34	2.82	−2.57	0.75	0.25	0.01
(CI_{95})	(±0.50)	(±0.16)	(±0.57)	(±0.55)	(±0.51)	(−)

Following the Buckingham π theorem, multiple non-dimensional groups can be formed out of these five dimensional parameters. Hence, grouping these parameters can be done in numerous different ways and the chosen groups are based upon sensible assumptions. Using the coefficients in table 1, it is reasonable to combine the velocity perturbations and the mean incoming flow velocity as u'/U_∞. Further, the excitation frequency and natural shedding frequency can be coupled as $(f_e/f_0)^{-2.57}$. Using these choices, the scaling equation simplifies to:

$$\frac{u'}{U_\infty} = 0.34\left(\frac{f_e}{f_0}\right)^{-2.57} {f_0}^{0.25} {U_\infty}^{-0.25} {d_c}^{0.25}. \tag{3}$$

This indicates the emergence of another non-dimensional frequency term in comparison to equation 1. Since the coefficients are the same, the remaining dimensional parameters can be grouped together to form the cylinder based Strouhal number, as $(f_0 d_c/U_\infty)^{0.25}$. The final form of this data-driven model is shown in equation 4 and a subsequent comparison between predicted values and experimentally measured values of u'/U_∞ displays good agreement (figure 3(b)). This novel data-driven model reveals that in addition to f_e/f_0, the value of u'/U_∞ at which lock-in begins also depends on the Strouhal number. This is because the Strouhal number is not a constant value, but rather, it denotes a range of values which depend on the diameter of the cylinder. Using equation 4, it becomes possible to predict the velocity fluctuations required to induce lock-in given the cylinder diameter, the freestream velocity, the natural shedding frequency of the cylinder at that velocity and the excitation frequency.

$$\frac{u'}{U_\infty} = 0.34\left(\frac{f_e}{f_0}\right)^{-2.57}\left(\frac{f_0 d_c}{U_\infty}\right)^{0.25}. \tag{4}$$

Flowfield during vortex lock-in

While the scaling in equation 4 provides a reliable approach to determine the onset of lock-in, the composition of the non-dimensional groups also assist in interpreting the flow field during lock-in. Firstly, the emergence of the Strouhal number can be associated to the vortex shedding with a steady flow, which usually takes the form of the classical Kármán vortex street (2S mode). Secondly, at the point of lock-in, since $f_s = \frac{1}{2} f_e$, equation 4 can be rearranged to include the actual shedding frequency of the cylinder, f_s:

$$\frac{u'}{U_\infty} = 0.34\left(\frac{2f_s}{f_0}\right)^{-2.57}\left(\frac{f_0 d_c}{U_\infty}\right)^{0.25}. \tag{5}$$

The rearranged equation 5 reveals that at the point of lock-in, the shedding frequency (f_s) is also an important parameter which can be linked to the vortex patterns formed when the oscillating component of the flow becomes substantial. Although it may not be instinctive to expect the shedding pattern to change from an instant to another, figures 4(a) and 4(b) confirms that it is possible to achieve different modes of shedding, i.c. 2S and 2P, at the same phase of the excitation cycle. Figures 4(a) and 4(b) depict the most dominant modes observed

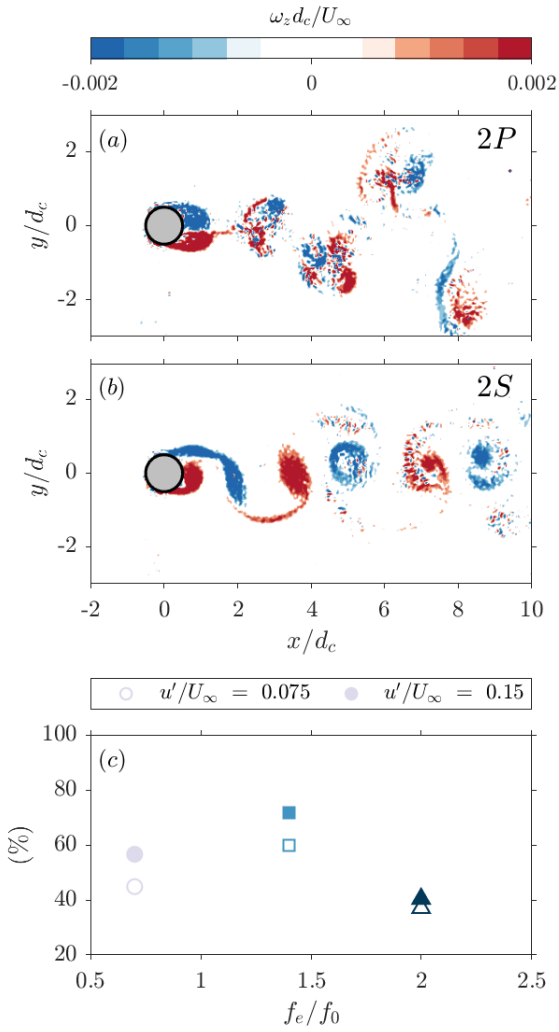

Figure 4. Contour plot of the normalised vorticity for instantaneous snapshots within the same phase of an actuation cycle denoting the occurrence of bimodal behaviour with (a) symmetric mode with a 2P vortex pattern and (b) alternating mode with a 2S vortex pattern. (c) Number of occurence of the symmetric mode across all phases as f_e/f_0 and u'/U_∞ are varied.

in the flowfield at the point of lock-in. These were the symmetric mode, characterised by the 2P shedding pattern, and the alternating mode, characterised by the 2S mode. It was observed that these two modes competed against each other and the switch from one mode to another was random across all phases and all cases. Such a bimodal nature of the shedding is consistent with the findings of Konstantinidis *et al.* (2007). However, this also implies that the low speed PIV data is extraneous since phase locking is only meaningful for those conditions where the vortex roll-up or vortex shedding is synchronised with the imposed perturbation. However, a statistical analysis of the vortex shedding patterns present in all instantaneous snapshots is still valid.

Hence, the probability of occurrence of these two types of vortex shedding pattern was computed across all the cases (figure 4(c)). Firstly, a general trend is that the percentage of snapshots with the symmetric mode is consistently higher at a large value of u'/U_∞ compared to a lower value, across the whole range of f_e/f_0. This is expected since the induced perturbation is purely symmetric and any increase in amplitude will amplify the energy transfer between the flow and the cylinder, which enhances the symmetric nature of the vortex roll-up and shedding. Additionally, the percentage of snapshots with 2P mode initially increases with f_e/f_0 up to a value of 1.5, after which a slump is observed at f_e/f_0 of 2.0. Konstantinidis *et al.* (2007) explained that a vortex must have achieved a certain critical strength before shedding. In an acoustically-driven oscillatory flow, sound energy is fed into the shedding process by superposition and this leads to an increase in circulation. When f_e/f_0 is less than 2.0, the vortex shedding frequency, f_s, is less than f_0, i.e. the vortex has more time to develop. Thus, each vortex accumulates more vorticity than a single vortex can handle, thereby leading to a redistribution into several vortices which are shed as pairs in the 2P mode. This also occurs when the amplitude of the perturbation is higher and justifies the higher percentage of snapshots with the symmetric mode. At f_e/f_0 of 2.0, our findings show that there is minimal influence of the amplitude of perturbations on the probability of occurrence of the symmetric mode. Rather, the alternating mode is prevalent at f_e/f_0 of 2.0, similar to the observations of Konstantinidis & Balabani (2006).

Since the vortex roll-up and shedding is not phase-locked to the imposed perturbation, an analysis of the time-averaged flow features is deemed more sensible. In particular, the wake properties behind the cylinder at various lock-in locations is inspected. Distribution of the mean and r.m.s velocity values along the wake centerline for selected cases are shown in figures 5(b) and 5(c). The general trend in the mean velocity profile is the existence of a peak velocity deficit value downstream of the cylinder, after which the velocity increases asymptotically. The results show that the time-averaged wake structure is modified in a systematic manner as the f_e/f_0 is varied across the lock-in range. Griffin (1995) defined the formation length of the recirculation bubble as the location of the peak in velocity fluctuations. Both the peak in velocity deficit and the peak in velocity fluctuations follow the same trend. As f_e/f_0 increases, the location of the peak moves closer to the cylinder which not only implies that the recirculation bubble is shortening, but also that vortex roll-up and shedding occurs closer to the cylinder. Analysis of the r.m.s profiles further indicates that higher amplitudes of perturbations result in higher $u_{r.m.s}/U_\infty$ and shorter wakes.

CONCLUSION

A parametric study was conducted in order to investigate the concept of vortex lock-in for circular cylinders in an oscillatory flow. Cylinders of various diameters were positioned at the velocity node and velocity anti-node in a standing wave, and hot-wire anemometry was performed to determine the dominant frequencies present in the flowfield. Planar PIV measurements were subsequently carried out for selected cases in order to better understand the physical mechanisms driving lock-in.

The results demonstrated good agreement with previous findings of Barbi *et al.* (1986) and the significance of the velocity perturbations was also established by comparing the shedding frequency at the velocity anti-node and velocity node. This led to the derivation of a novel scaling based on the experimental data, which encapsulates both the fluidic properties of the flow and the geometrical properties of the cylinder. This newly established data-driven model allows the prediction of the flow perturbations required to trigger lock-in, given the cylinder diameter, excitation frequency, steady mean velocity and the corresponding natural shedding frequency are known. The model and experimental data showed good agree-

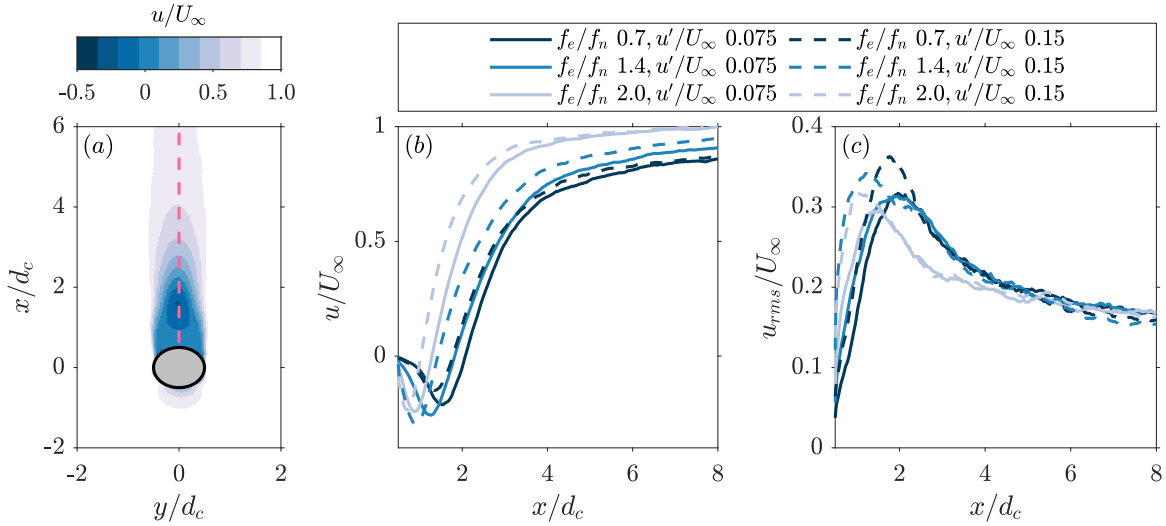

Figure 5. (a) Contour plot of the time-averaged streamwise velocity for f_e/f_0 of 0.7 and u'/U_∞ of 0.075. The pink dotted line represents the location across which the profiles are taken. Note that for brevity, only one case is shown here. (b) Distribution of the mean streamwise velocity along the wake centerline for various combinations of f_e/f_0 and u'/U_∞. (c) Distribution of the r.m.s fluctuation of the streamwise velocity across the wake centerline for various combinations of f_e/f_0 and u'/U_∞.

ment with an r.m.s error of only 0.01. The scaling established the Strouhal number of the cylinder as an important parameter, even at the point of lock-in. The non-dimensional parameters established by the scaling were also used to provide an explanation for the bimodal nature of the vortex shedding, as observed from PIV measurements. Statistical analysis of the vortex shedding patterns was carried out and the time-averaged wake properties were assessed, with any sensitivity on the flow perturbations and/or f_e/f_0 discussed.

Acknowledgement

The authors acknowledge funding from the Research Council of Norway (FRIPRO), project 299946.

REFERENCES

Al-Mdallal, Q.M., Lawrence, K.P. & Kocabiyik, S. 2007 Forced streamwise oscillations of a circular cylinder: Locked-on modes and resulting fluid forces. *Journal of Fluids and Structures* **23** (5), 681–701.

Balachandar, S., Mittal, R. & Najjar, F. M. 1997 Properties of the mean recirculation region in the wakes of two-dimensional bluff bodies. *Journal of Fluid Mechanics* **351**, 167–199.

Barbi, C., Favier, D. P., Maresca, C. A. & Telionis, D. P. 1986 Vortex shedding and lock-on of a circular cylinder in oscillatory flow. *Journal of Fluid Mechanics* **170** (1973), 527–544.

Blevins, R. D. 1985 The effect of sound on vortex shedding from cylinders. *Journal of Fluid Mechanics* **161** (1), 217.

Detemple-Laake, E. & Eckelmann, H. 1989 Phenomenology of Kármán vortex streets in oscillatory flow. *Experiments in Fluids* **7** (4), 217–227.

Griffin, Owen M. 1995 A note on bluff body vortex formation. *Journal of Fluid Mechanics* **284**, 217–224.

Hall, J.W., Ziada, S. & Weaver, D.S. 2003 Vortex-shedding from single and tandem cylinders in the presence of applied sound. *Journal of Fluids and Structures* **18** (6), 741–758.

Jankee, Girish K & Ganapathisubramani, Bharathram 2021 Scalings for rectangular synthetic jet trajectory in a turbulent boundary layer. *Journal of Fluid Mechanics* **915**, A57.

Konstantinidis, E & Balabani, S 2006 Symmetric vortex shedding from a circular cylinder under periodic flow forcing. In *Proceedings of PVP2006-ICPVT-11 ASME Pressure Vessels and Piping Division Conference*. Vancouver, British Columbia, Canada.

Konstantinidis, E. & Balabani, S. 2007 Symmetric vortex shedding in the near wake of a circular cylinder due to streamwise perturbations. *Journal of Fluids and Structures* **23** (7), 1047–1063.

Konstantinidis, E., Balabani, S. & Yianneskis, M. 2005 The timing of vortex shedding in a cylinder wake imposed by periodic inflow perturbations. *Journal of Fluid Mechanics* **543** (1), 45.

Konstantinidis, Efstathios, Balabani, Stavroula & Yianneskis, Michael 2007 Bimodal vortex shedding in a perturbed cylinder wake. *Physics of Fluids* **19** (1), 011701.

Konstantinidis, Efstathios & Liang, Chunlei 2011 Dynamic response of a turbulent cylinder wake to sinusoidal inflow perturbations across the vortex lock-on range. *Physics of Fluids* **23** (7).

Ongoren, A. & Rockwell, D. 1988 Flow structure from an oscillating cylinder Part 2. Mode competition in the near wake. *Journal of Fluid Mechanics* **191** (1), 225.

Seybert, A. F. & Ross, D. F. 1977 Experimental determination of acoustic properties using a two-microphone random-excitation technique. *The Journal of the Acoustical Society of America* **61** (5), 1362–1370.

Sumner, D. 2010 Two circular cylinders in cross-flow: A review. *Journal of Fluids and Structures* **26** (6), 849–899.

Williamson, C. H. K. 1985 Sinusoidal flow relative to circular cylinders. *Journal of Fluid Mechanics* **155** (December), 141–174.